Biochemical and Biophysical Research Communications 424 (2012) 290–294

Contents lists available at SciVerse ScienceDirect

Biochemical and Biophysical Research Communications

journal homepage: www.elsevier.com/locate/ybbrc

C-terminal truncation of Vascular Endothelial Growth Factor mimetic helical peptide preserves structural and receptor binding properties

Barbara Ziaco [a], Donatella Diana [a], Domenica Capasso [b], Rosanna Palumbo [a], Veronica Celentano [a], Rossella Di Stasi [a], Roberto Fattorusso [c], Luca Domenico D'Andrea [a,*]

[a] Istituto di Biostrutture e Bioimmagini, CNR, Via Mezzocannone 16, 80134 Napoli, Italy
[b] Facoltà di Scienze Biotecnologiche, Università di Napoli "Federico II", Via Mezzocannone 16, 80134 Napoli, Italy
[c] Dipartimento di Scienze Ambientali, Seconda Università di Napoli, Via Vivaldi 46, 81100 Caserta, Italy

ARTICLE INFO

Article history:
Received 21 June 2012
Available online 27 June 2012

Keywords:
Peptide
Helix
NMR
VEGF
Conformational analysis

ABSTRACT

Vascular Endothelial Growth Factor mimetic peptides have interesting applications in therapeutic angiogenesis. Recently, we described the proangiogenic properties of a 15 mer peptide designed on the N-terminal helix 17–25 of VEGF. The peptide was stabilized introducing well known peptide chemical tools among which N- and C-terminal capping sequence. Here, we show that the C-terminal sequence does not affect the structural and biological properties of the full-length peptide. In fact, a C-terminal truncated analog peptide resulted in a well folded and stable helix retaining the ability to bind to VEGF receptors. This study will allow to develop smaller peptidomimetic analogs able to modulate the VEGF-dependent angiogenesis.

1. Introduction

In the last years many novel molecules able to modulate the angiogenesis targeting Vascular Endothelial Growth Factor (VEGF) receptors have been described [1–4]. VEGF receptors (VEGFR1 and VEGFR2) belong to the family of tyrosine kinase receptors and they are mainly exposed on the surface of endothelial cells (ECs). VEGF binding induces receptor dimerization and autophosphorylation which trigger the intracellular signaling ending in endothelial cells activation [5].

Chemical compounds targeting VEGF receptors are interesting for several pharmaceutical applications. For example, molecules with anti-angiogenic activity may find application to treat diseases such as cancer, age-related macular diseases, and arthritic rheumatoid [3,6,7]; molecules with a pro-angiogenic activity are useful in therapeutic angiogenesis [7,8]. Finally, molecules interacting with high affinity and specificity to the extracellular domain of VEGF receptors can be employed as targeting agents for the molecular imaging of angiogenesis [9,10].

We described the design, biological and structural characterization of a helical peptide targeting VEGF receptors [11]. The 15-mer peptide, QK, was designed on the N-terminal helix 17–25 of VEGF which is involved in receptor recognition [12]. The VEGF interacting residues were conserved and the helical conformation was stabilized introducing peptide chemical tools among which N- and C-terminal capping sequence. NMR conformation analysis of QK revealed that it adopts a well-defined helical conformation in aqueous solution; furthermore, it was demonstrated that QK has the same biological properties of VEGF *in vitro* [11,13] and *in vivo* [14,15] resulting one of few synthetic molecules able to activate VEGF receptors [11,16,17]. Recently, the peptide QK has been used to decorate biomaterial scaffolds [18–24] for application in tissue regeneration. Peptide QK shows an unusual thermal stability retaining at high temperature about the 80% of its secondary structure as ascertained by NMR spectroscopy and MD simulations [25]. We demonstrated that this behavior can be in part attributed to the high tendency of N-terminal residues to adopt a helical turn in the first events of the folding, and to an intramolecular *i, i* + 3 contact between the side chain of the two leucine residues [25,26]. Finally, circular dichroism analysis suggested that the peptide QK_{1-12}, a QK analog, which presents the deletion of the C-terminal region, could retain the helical conformation [25].

In this study we explore the role of the QK C-terminal region on peptide structure, conformational stability and biological activity. In particular, we report the conformational and thermal analysis in aqueous solution of QK_{1-12} by means of circular dichroism and NMR spectroscopies. Furthermore, the ability of QK_{1-12} to bind to VEGFR1 was tested to verify whether peptide QK_{1-12} retains QK receptor binding properties.

The correlation between peptide structure and QK bioactivity will be useful to develop smallest peptidomimetic analogs able to modulate the VEGF-dependent angiogenesis.

* Corresponding author.
E-mail address: ldandrea@unina.it (L.D. D'Andrea).

0006-291X/$ - see front matter © 2012 Elsevier Inc. All rights reserved.
http://dx.doi.org/10.1016/j.bbrc.2012.06.109

2. Materials and methods

2.1. Peptide synthesis

Peptides QK (Acetyl-KLTWQELYQLKYKGI-amide), QK_{1-12} (Acetyl-KLTWQELYQLKY-amide) and QK_{4-15} (Acetyl-KWQELYQLKYKGI-amide) were synthesized using standard procedure as previously reported [24]. Peptides were biotinylated on solid phase reacting the peptide N^{α} amino group, after Fmoc deprotection, with 3 eq of N-(+)-biotinyl-6-aminocaproic acid (Sigma–Aldrich, Milan, Italy), 3 eq of HATU and 6 eq of DIPEA in DMF for 3 h at room temperature under shaking.

Peptide purifications were carried out on a Shimadzu LC-8A, equipped with a SPD-M10 AV detector using a C12 column Jupiter Proteo (250 × 10 mm, 90 Å, 10 μm; Phenomenex, Torrance, US). Peptide analysis and identification was performed on the LC–MS LCQ Deca XP MAX (Thermo Fisher Scientific, Waltham, US) equipped with an ESI source and ion trap mass analyzer coupled to a Surveyor HPLC system (with photo diode array detector) using a C12 column Jupiter Proteo (50 × 2 mm, 90 Å, 4 μm; Phenomenex, Torrance, US). All peptides were afforded in high pure and homogenous forms as assessed by analytical RP-HPLC (>95% based on the profile at 210 nm). Analytical data are reported in Table S1 of Supplementary data.

2.2. Circular dichroism spectroscopy

Far-UV circular dichroism spectra were recorded on a J-810 spectropolarimeter (Jasco, Easton, US), equipped with a PTC-423S/15 Peltier temperature controller, using a 0.1 cm quartz cell (Hellma, Milan, Italy) in the range 190–260 nm. Peptides were dissolved in 10 mM phosphate buffer, pH 7.1 at a concentration of 50 μM. Spectra were acquired using a band width of 1 nm, a response time of 8 s, a data pitch of 0.1 nm and a scanning speed of 10 nm/min. Each spectrum was the average of three scans with the background of the buffer solution subtracted. CD data were expressed as mean residue ellipticity (θ). Spectra were processed using the Spectra Manager software. Peptide concentration was determined by absorption spectroscopy on a Jasco (Easton, USA) V-550 UV–VIS spectrophotometer using 1 cm path length quartz cell (Hellma, Milan, Italy) and an absorption coefficient at 280 nm of 8480 M^{-1} cm^{-1} in water [27].

2.3. Nuclear magnetic resonance spectroscopy

NMR spectroscopic samples were prepared by dissolving the lyophilized peptide (~1 mg) in (H_2O/D_2O 9:1 v/v, 0.6 ml). The NMR spectra were acquired on a Varian INOVA 600 MHz spectrometer equipped with a cold probe. Data acquisition for homonuclear 2D-TOCSY and 2D-NOESY spectra of QK_{1-12} were carried out at 298 K with a mixing time of 70 ms and 250 ms respectively. Double quantum filtered spectroscopy (DQF-COSY) was recorded with 4096 data points in the direct dimension and with 500 increments each comprising 64 scans to obtain enough resolution to measure the $^3J_{HNH\alpha}$ coupling constants. All spectra were processed with software Sparky [28] and analyzed with Neasy [29], a tool of computer aided resonance assignment (CARA) software.

The diffusion-ordered NMR spectroscopy (DOSY) [30] was carried out as previously reported [25,26]. The three-dimensional structures were determined by combined automated NOESY cross-peak assignment [31] and structure calculation with torsion angle dynamics implemented in the program CYANA [32]. The color figures and the structure analysis have been performed with the program MOLMOL [33].

Thermal unfolding of QK_{1-12} peptide was studied by 2D-TOCSY acquired at 298, 303, 308, 313, 318, 323, 328, 333, 338 and 343 K. All spectra were acquired consecutively. NMR experiments were carried out on a Varian Inova 400 MHz spectrometer, where the probe temperature was regularly calibrated by using methanol and ethylenglycol [34].

2.4. Cell culture

The human melanoma A375 cell line was a gift from Dr. L. Aloj (Istituto Nazionale Tumori, Fondazione G. Pascale, Napoli, Italy). The cells were maintained in DMEM, supplemented with 10% heat-inactivated FCS, 2 mM L-glutamine and grown at 37 °C in a humidified 5% CO_2 atmosphere. A375 cells were detached by incubation with 50 mM EDTA in PBS, centrifuged, and suspended in PBS containing 0.1% BSA.

2.5. Flow cytometry

Cell aliquots (1×10^5) were incubated at 4 °C in 100 μL final volume. At the end of the incubation, cells were pelleted, washed, resuspended in 0.1% BSA/PBS to 400 μL and analyzed using a flow cytometer equipped with a 488 nm argon laser (FACScan, Becton Dickinson, CA, USA). A total of 20,000 events per sample were collected. Values of fluorescence intensity were obtained from histogram statistic of CellQuest software.

For binding experiments, cells were incubated with biotinylated peptides at different concentration. After 1 h the cells were treated with FITC-avidin for additional 30 min. The fluorescence intensity of untreated cells was comparable to biotin labeled QK_{4-15} treated cells. Therefore, cells treated with 10 μM biotin QK_{4-15} were used as negative control. For competitive binding A375 were incubated with different concentrations of QK_{1-12} and 200 μM QK_{4-15} for 1 h. After washing with 0.1% BSA/PBS, the cells were incubated with 25 nM biotin labeled VEGF for 30 min. Finally the cells were treated with FITC-conjugated avidin for other 30 min. Cell suspensions incubated with 25 nM biotin labeled VEGF were used as positive control. The experiment was performed at least 3 times.

2.6. Statistical analysis

Data are represented as means ± SD from at least three independent experiments. Differences between the groups were determined by one way ANOVA using the GraphPad Prism version 5.00 for Windows (GraphPad Software, San Diego California USA). Dunnett's post test was performed for evaluation of differences between the groups. A value of $P < 0.05$ was considered to indicate a significant difference between groups.

3. Results

3.1. Circular dichroism studies

Peptides QK_{1-12} and QK showed similar CD spectra characterized by a double negative minima at 208 and 222 nm, a positive maximum around 195 nm, a crossover point around 200 nm, and a comparable overall helical content [25]. Peptides were titrated with increasing concentration of TFE to evaluate their propensity to adopt a full helical conformation. Increasing TFE concentration CD spectra of both peptides showed deeper minima, a significant enhancement of the positive maximum and the shift of the crossover point towards 200 nm, indicating an increasing of the overall helical content (Figure S1). The ellipticity ratio ($\theta_{222}/\theta_{208}$) is constant (around 0.8) along the titration for both peptides. Furthermore, QK and QK_{1-12} TFE titrations showed an isodicroic point at

203 nm suggesting a two-state equilibrium between α-helix and random coil conformations.

We already reported that QK peptide, which is monomeric in the experimental condition tested, is characterized by an unusual thermal stability [24]. Then, we verified if C-terminus deletion will affect the QK thermal stability. Thermal unfolding of peptide QK_{1-12}, monitored at 222 nm (θ_{222}), showed a profile (Figure S2) comparable with QK [25]. In detail, QK_{1-12} showed a relevant thermal stability retaining the 65% of its room temperature helical content at 343 K; however, it resulted slight less thermal stable than QK which, at the same temperature, retained the 79% of its room temperature helical content [25]. It is evident from the CD analysis that the two peptides displayed very similar conformational properties, suggesting that the truncation of the C-terminal tail is not affecting the overall structure of QK peptide, but slightly reduces the thermal stability of QK peptide.

3.2. NMR conformational analysis

To gain a deeper insight on the molecular behavior of QK_{1-12}, a conformational analysis in aqueous solution of peptide QK_{1-12} was performed by NMR. The aggregation state of QK_{1-12} peptide was determined by Diffusion-Ordered SpectroscopY (DOSY) experiments performed under conditions identical to those used for the NMR structure determination. DOSY measurements (Figure S3) provided a diffusion coefficient value of of $2.30 \times 10^{-10}\ m^2 s^{-1}$, which corresponds to what is expected for a monomeric 12-mer helical peptide in water solution [25,26,35]. Identification of spin systems and assignment of individual resonances for QK_{1-12} were established by a combination of DQF-COSY and TOCSY spectra and sequence-specific assignment was obtained by NOESY experiment (Figure S4). Proton chemical shifts and $^3J_{HNH\alpha}$, extracted from the DQF-COSY spectrum, are listed in Table S2 in the Supplemental data. The H_α chemical shifts analysis, performed by Chemical Shift Index [36], strongly indicated the presence of a helical structure encompassing the residue 4–12 (Fig. 1). The NOESY assignments of the QK_{1-12} peptide were based on a high number of sequential and medium range NOEs. In particular sequential H_α–$H_N(i, i+1)$ and H_N–$H_N(i, i+1)$ NOE connectivity, as well as medium range H_α–$H_N(i, i+3)$ and H_α–$H_\beta(i, i+3)$ NOE connectivity, primarily observed in the 4–12 region of the peptide, as showed in Figure S5, confirmed the high helical propensity of the central region of QK_{1-12}, as already indicated by the Chemical Shift Index analysis. For the structure refinement, the final input file for the CYANA structure calculation software contained 109 meaningful distance constraints (42 intra-residue, 38 short- and 29 medium-range) and 58 angle constraints which were derived from intra-residue and sequential NOEs and the $^3J_{HNH\alpha}$ coupling constants through the GRIDSEARCH module. NMR structural statistics are shown in Table 1. Initially, 100 random structures were generated by CYANA.

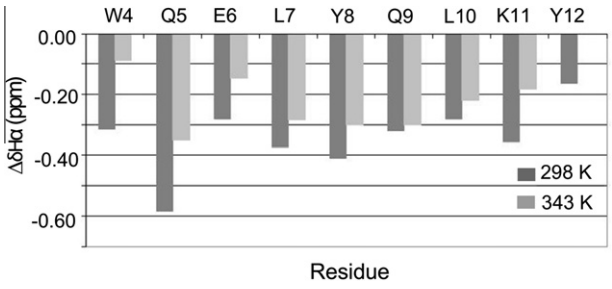

Fig. 1. H_α chemical shift deviations from random coil values ($\Delta\delta H_\alpha$) of the QK_{1-12} at 298 and 343 K. The continuous line at 0.1 ppm represents the CSI threshold for amino acid in helical conformation.

Table 1
NMR structural statistics of peptide QK_{1-12}.

Quantity	Value
NOEs upper distance limit	109
Intra-residue	42
Short-range	38
Medium- and Long-range	29
Dihedral angle constraints	58
Residual target function, Å	0.11 ± 0.02
Residual NOE violations	
Number > 0.1 Å	±1
Maximum, Å	0.17 ± 0.02
Residual Angle violations	
Number > 2.0°	0 ± 0
Maximum, °	0
Amber energies, kJ/mol	
Total	−388 ± 18
Van der Waals	−131 ± 11
Electrostatic	−200 ± 20
RMSD to the mean coordinates, Å	
N, Cα, C′ (4..12)	0.12 ± 0.01
All heavy atoms (4..12)	0.98 ± 0.03

The 20 conformations with the lowest target function values were chosen for the further refinement using restrained energy minimization. The backbone superposition of the final 20 structures is shown in Fig. 2A; the whole range of structures was helix shaped with a good pairwise RMSD for the backbone atoms and all heavy atoms of the mean structure, 0.12 ± 0.01 and 0.98 ± 0.03 Å, respectively.

The NMR solution structure of the QK_{1-12} peptide at 298 K is almost identical to that of QK consisting of a well-defined helix encompassing residues 4–12, as showed by the backbone superposition (RMSD 0.88 Å) of the QK_{1-12} and the QK representative structures (Fig. 2B). Interestingly, C-terminal truncation does not affect QK helical length, being Tyr12 the last residue in helical conformation in both peptides (Fig. 2B). Notably the C-terminal unstructured end, reported for QK [11], is absent in QK_{1-12} (Fig. 2B). Remarkably, the well-defined helical conformation of QK_{1-12} in aqueous solution is quite unusual for a short peptide (12 mer) and has been reported only for peptides with unnatural constraints or in organic solvents.

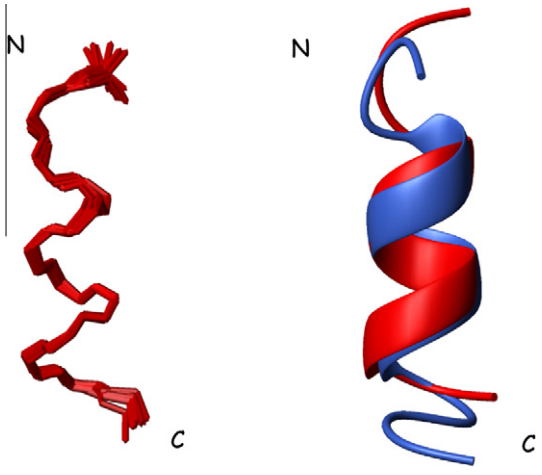

Fig. 2. NMR structure of peptide QK_{1-12}. (A) Backbone superposition of the 20 minimum energy structures of QK_{1-12} (RMSD = 0.12 ± 0.01 Å; fitting residues 4–12). (B) Backbone superposition of the representative NMR structures of the QK_{1-12} (red) and QK (blue) peptides (RMSD = 0.88 ± 0.05 Å) (For interpretation of the references to colour in this figure legend, the reader is referred to the web version of this article.).

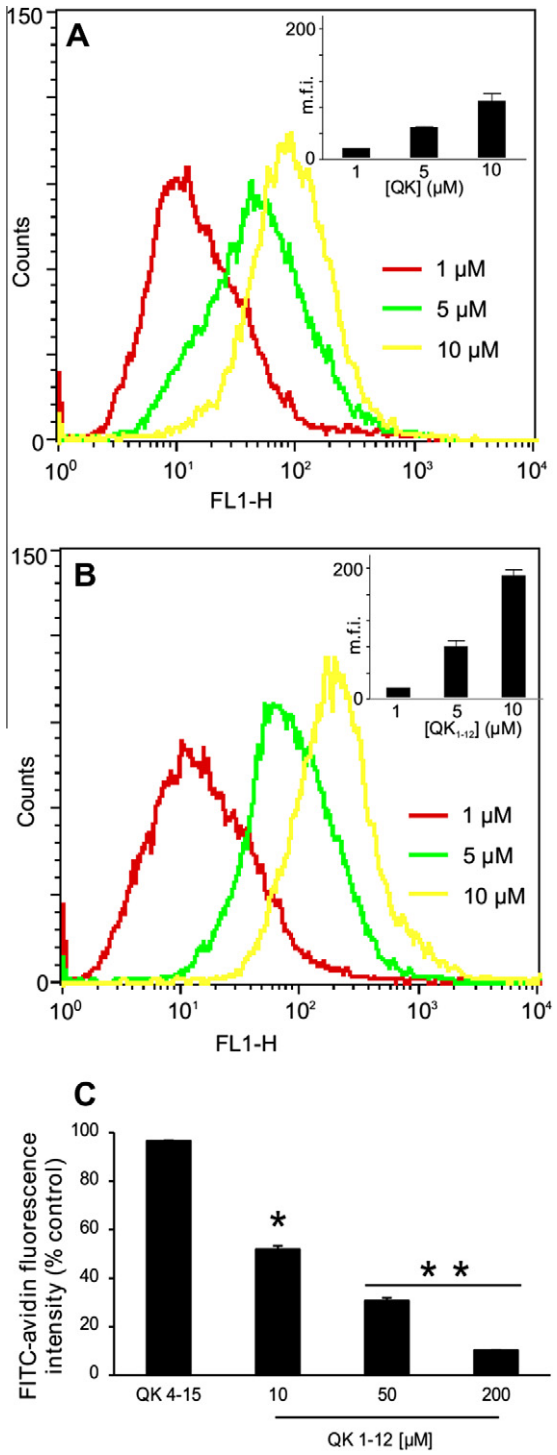

Fig. 3. Flow cytometric analysis of binding of QK (A) and QK_{1-12} (B) to A375 cells. Cells at a density of 1×10^6 cells/mL were incubated with biotinylated peptides at different concentrations for 1 h at 4 °C. Cells treated with biotinylated QK_{4-15} were used as negative control. The fluorescence emitted by negative control cells was used to set a threshold gate. The mean fluorescence intensity (m.f.i.) for each concentration of peptide is given in the top right corner. Values of fluorescence intensity were obtained from histogram statistic of CellQuest software. (C) Inhibition of biotinylated VEGF binding to A375 cells by increasing concentrations of QK_{1-12} peptide. After preincubation with QK_{1-12} or QK_{4-15} peptides for 1 h at 4 °C, cells were treated with 25 nM biotin VEGF (positive control), then the fluorescence intensity was measured upon addition of FITC-avidin. Results are expressed as the percentage of FITC-avidin fluorescence bound to the cell compared to positive control. Date points represent means ± SD of three independent experiments. $^*P < 0.05$; $^{**}P < 0.001$.

To investigate the QK_{1-12} thermal stability, a set of 2D-TOCSY NMR spectra were recorded every 5 K in the temperature range 298–343 K and proton chemical shifts were assigned. In particular, H_α chemical shifts, which have proven to be the most sensitive probe to follow the conformational changes of the peptides [36], have been employed to obtain higher resolution structural details of the thermal dependence of the QK_{1-12}. As showed in Fig. 1, the chemical shift index (CSI) analysis showed a continuous stretch of negative values ($\Delta\delta H\alpha > 0.1$ ppm) encompassing residues 4–12, suggesting that also QK_{1-12} peptide is predominantly in helical conformation at high temperature. In particular, QK_{1-12} showed at 343 K a 40% helicity decrease with respect to its room temperature as estimated by $\Delta\delta H\alpha$ measurements. The CSI analysis showed that the QK_{1-12} helical structure is present at 343 K (Fig. 1), even though it is reduced to residues 5–11. This high thermal structural stability is in agreement with the observation that QK maintains residues 4–11 in helical structure at 343 K [25], nonetheless it appears very surprising for a 12-mer helical peptide. Comparison of the QK and QK_{1-12} thermal stability confirms the fundamental role of the N-terminus in stabilizing QK helical structure as demonstrated previously on the basis of biochemical, NMR and computational studies [25,26].

3.3. VEGFR1 binding studies

QK exerts its biological activity on endothelial cells through binding cell surface VEGF receptors. We showed that QK activity depends on its structural properties [11]. Truncation of the C-capping region left QK conformation and structural properties unaffected, as binding residues were not modified, QK and QK_{1-12} should share the same biological activity. To verify this hypothesis we performed a cell binding assay by flow cytometry on A375 melanoma cell line which express VEGFR1 receptor on its surface. The ability of biotinylated QK and QK_{1-12} peptides to recognize cell surface VEGFR1 was demonstrated measuring the fluorescence intensity of the cells at different peptide concentrations (Fig. 3). The two peptides showed a shift to greater fluorescence intensity in a dose-dependent manner suggesting a specific binding to A375 cells. Peptide QK_{4-15}, which lacks of the N-capping region and is unordered in solution [25], was used as negative control and it was unable to bind to A375 cells. Moreover, cells treated with QK_{1-12} (Fig. 3B) showed a shift to greater fluorescence intensity compared to cells incubated with QK (Fig. 3A) suggesting that the more compact structure would affect the binding affinity towards cell surface receptors. To verify that peptide binding to cell was mediated by VEGFR1 receptors we incubated A375 cells with biotinylated VEGF and increasing concentrations of peptide QK_{1-12} (Fig. 3C). The positive control value was defined as the fluorescence of 25 nM VEGF bound to the cells in absence of peptide. VEGF binding to VEGFR1 was reduced as the concentration of QK_{1-12} peptide increased. Notably, the fluorescence intensity was reduced to a maximum of 10% of positive control in presence of 200 μM peptide (Fig. 3C). In contrast, 200 μM QK_{4-15} were unable to reduce VEGF binding to A375 cells. This data suggests that QK_{1-12} and VEGF compete for the same sites on the surface of A375 cells which could reasonably identified in VEGFR1.

Overall the biological data confirmed that peptide QK_{1-12} is able to bind VEGFR1 receptors as its parent peptide QK and suggests that truncation of QK C-terminal tail leaves unaffected QK biological properties.

4. Discussion

QK is a one of the few VEGF mimetic peptides with proangiogenic activity. It showed favorable properties in wound healing

[13–15] and tissue engineering [18–24] applications. QK was designed from scratch, based on the X-ray structure of the complex VEGF-VEGFR1$_{D2}$, keeping fixed the tridimensional arrangements of the interacting residues and stabilizing the helical conformation [11]. The C-terminal sequence, Lys-Gly-Ile, was inserted as C-capping tool and was modeled on the Schelling motif [37].

We were interested in analyzing the contribution of the C-terminal sequence Lys-Gly-Ile to QK peptide structure, conformational stability and biological activity. Previously, we showed that QK bioactivity is correlated to its helical structure. In fact, a peptide reproducing the VEGF sequence 17–31, VEGF15, which is unstructured in solution, does not show any biological activity even if all the interacting residues are conserved suggesting a fundamental role for peptide preorganization [11]. Based on the CD analysis we suggested [25] that peptide QK$_{1-12}$ should retain the QK biological activity; on the contrary, peptide QK$_{4-15}$ should be biological inactive, as it is unstructured in solution as a consequence of the deletion of the N-terminal region, which is involved in peptide folding and stability [25].

In this study we demonstrate that truncation of the C-capping region of QK does not significantly affect its tridimensional structure and only moderately reduces its thermal stability. As matter of fact, QK$_{1-12}$ is a well folded helical peptide which mostly retains its structure at 343 K. Interestingly, the NMR structure showed that QK$_{1-12}$ in aqueous solution lacks of C-terminal disordered region resulting in a more compact structure than QK, thus representing one of shortest helical peptide composed of all natural amino acids. Accordingly, QK$_{1-12}$ retains the ability of QK to bind to VEGFR1 suggesting a similar biological activity, differently from peptide QK$_{4-15}$ which does not bind to VEGFR1 as expected.

In conclusion, the C-terminal sequence does not affect the structural and biological properties of peptide QK. The C-terminal truncated analog peptide assumes in solution a well folded and stable helix and retains the ability to bind to VEGF receptors. This information will be useful towards the development of a peptidomimetic analog of peptide QK.

Acknowledgments

This research was supported by MIUR-PON 2007-2013 (PON 01_2388). We would like to thank L. De Luca and L. Zona for technical assistance.

Appendix A. Supplementary data

Supplementary data associated with this article can be found, in the online version, at http://dx.doi.org/10.1016/j.bbrc.2012.06.109.

References

[1] L.D. D'Andrea, A. Del Gatto, C. Pedone, E. Benedetti, Peptide-based molecules in angiogenesis, Chem. Biol. Drug Des. 67 (2006) 115–126.
[2] J. Folkman, Angiogenesis, Annu. Rev. Med. 57 (2006) 1–18.
[3] A. Grothey, E. Galanis, Targeting angiogenesis: progress with anti-VEGF treatment with large molecules, Nat. Rev. Clin. Oncol. 6 (2009) 507–518.
[4] L.D. D'Andrea, A. Del Gatto, L. De Rosa, et al., Peptides targeting angiogenesis related growth factor receptors, Curr. Pharm. Des. 15 (2009) 2414–2429.
[5] N. Ferrara, H.P. Gerber, J. LeCouter, The biology of VEGF and its receptors, Nat. Med. 9 (2003) 669–676.
[6] J. Folkman, Angiogenesis: an organizing principle for drug discovery?, Nat Rev. Drug Discov. 6 (2007) 273–286.
[7] N. Ferrara, R.S. Kerbel, Angiogenesis as a therapeutic target, Nature 438 (2005) 967–974.
[8] J. Jacobs, Combating cardiovascular disease with angiogenic therapy, Drug Discov. Today 12 (2007) 1040–1045.
[9] W. Cai, X. Chen, Multimodality molecular imaging of tumor angiogenesis, J. Nucl. Med. 49 (2008) 113S–128S.
[10] L.D. D'Andrea, A. Romanelli, R. Di Stasi, C. Pedone, Bioinorganic aspects of angiogenesis, Dalton Trans. 39 (2010) 7625–7636.
[11] L.D. D'Andrea, G. Iaccarino, R. Fattorusso, et al., Targeting angiogenesis: structural characterization and biological properties of a de novo engineered VEGF mimicking peptide, Proc. Natl. Acad. Sci. USA 102 (2005) 14215–14220.
[12] C. Wiesmann, G. Fuh, H.W. Christinger, et al., Crystal structure at 1.7 A resolution of VEGF in complex with domain 2 of the Flt-1 receptor, Cell 91 (1997) 695–704.
[13] F. Finetti, A. basile, D. Capasso, S. DiGaetano, R. Di Stasi, M. Pascale, C.M. Turco, M. Ziche, L. Morbidelli, L.D. D'Andrea, Functional and pharmacological characterization of a VEGF mimetic peptide on reparative angiogenesis, Biochem. Pharmacol. 84 (2012) 303–311.
[14] G.K. Dudar, L.D. D'Andrea, R. Di Stasi, et al., A vascular endothelial growth factor mimetic accelerates gastric ulcer healing in an iNOS-dependent manner, Am. J. Physiol. Gastrointest. Liver Physiol. 295 (2008) G374–381.
[15] G. Santulli, M. Ciccarelli, G. Palumbo, et al., In vivo properties of the proangiogenic peptide QK, J. Transl. Med. 7 (2009) 41–50.
[16] D. Diana, A. Basile, L. De Rosa, et al., β-hairpin peptide that targets vascular endothelial growth factor (VEGF) receptors: design, NMR characterization, and biological activity, J. Biol. Chem. 286 (2011) 41680–41691.
[17] S. Soro, A. Orecchia, L. Morbidelli, et al., A proangiogenic peptide derived from vascular endothelial growth factor receptor-1 acts through alpha5beta1 integrin, Blood 111 (2008) 3479–3488.
[18] G.A. Hudalla, W.L. Murphy, Biomaterials that regulate growth factor activity via bioinspired interactions, Adv. Funct. Mater. 21 (2011) 1754–1768.
[19] J.S. Lee, A.J. Wagoner Johnson, W.L. Murphy, A modular, hydroxyapatite-binding version of vascular endothelial growth factor, Adv. Mater. 22 (2010) 5494–5498.
[20] J.E. Leslie-Barbick, J.E. Saik, D.J. Gould, et al., The promotion of microvasculature formation in poly(ethylene glycol) diacrylate hydrogels by an immobilized VEGF-mimetic peptide, Biomaterials 32 (2011) 5782–5789.
[21] D. Suarez-Gonzalez, K. Barnhart, F. Migneco, et al., Controllable mineral coatings on PCL scaffolds as carriers for growth factor release, Biomaterials 33 (2012) 713–721.
[22] D. Suarez-Gonzalez, J.S. Lee, S.K. Lan Levengood, et al., Mineral coatings modulate β-TCP stability and enable growth factor binding and release, Acta Biomater. 8 (2011) 1117–1124.
[23] X. Wang, A. Horii, S. Zhang, Designer functionalized self-assembling peptide nanofiber scaffolds for growth, migration, and tubulogenesis of human umbilical vein endothelial cells, Soft Matter 4 (2008) 2388–2395.
[24] M.J. Webber, J. Tongers, C.J. Newcomb, et al., Supramolecular nanostructures that mimic VEGF as a strategy for ischemic tissue repair, Proc. Natl. Acad. Sci. USA 108 (2011) 13438–13443.
[25] D. Diana, B. Ziaco, G. Colombo, et al., Structural determinants of the unusual helix stability of a de novo engineered vascular endothelial growth factor (VEGF) mimicking peptide, Chem. Eur. J. 14 (2008) 4164–4166.
[26] D. Diana, B. Ziaco, G. Scarabelli, et al., Structural analysis of a helical peptide unfolding pathway, Chem. Eur. J. 16 (2010) 5400–5407.
[27] E. Gasteiger, C. Hoogland, A. Gattiker, et al., Protein identification and analysis tools on the ExPASy server, in: J.M. Walker (Ed.), The Proteomics Protocols Handbook, Humana Press, Totowa, 2005, pp. 571–607.
[28] T.D. Goddard, D.G. Kneller, SPARKY Version 3, University of California, San Francisco, California, US, 2001.
[29] J.E. Masse, R. Keller, AutoLink: automated sequential resonance assignment of biopolymers from NMR data by relative-hypothesis-prioritization-based simulated logic, J. Magn. Reson. 174 (2005) 133–151.
[30] K.F. Morris, G.S. Johnson, Diffusion-ordered two-dimensional nuclear magnetic resonance spectroscopy, J. Am. Chem. Soc. 114 (1992) 3139–3141.
[31] T. Hermann, P. Guntert, K. Wuthrich, Protein NMR structure determination with automated NOE assignment using the new software CANDID and the torsion angle dynamics algorithm DYANA, J. Mol. Biol. 319 (2002) 209–227.
[32] P. Guntert, C. Mumenthaler, K. Wuthrich, Torsion angle dynamics for NMR structure calculation with the new program DYANA, J. Mol. Biol. 273 (1997) 283–298.
[33] R. Koradi, M. Billenter, K. Wüthrich, MOLMOL: a program for display and analysis of macromolecular structures, J. Mol. Graphics 14 (1996) 51–55.
[34] M.L. Martin, J.J. Delpuech, G.J. Martin, Practical NMR Spectroscopy, Heyden, London, 1980.
[35] S. Yao, G.J. Howlett, R.S. Norton, Peptide self-association in aqueous trifluoroethanol monitored by pulsed field gradient NMR diffusion measurements, J. Biomol. NMR 16 (2000) 109–119.
[36] D.S. Wishart, B.D. Sykes, F.M. Richards, Relationship between nuclear magnetic resonance chemical shift and protein secondary structure, J. Mol. Biol. 222 (1991) 311–333.
[37] R. Aurora, G.D. Rose, Helix capping, Prot. Sci. 7 (1998) 21–28.